Parametrization of an anharmonic Kirkwood–Keating potential for $Al_xGa_{1-x}As$ alloys

Eunji Sim[a)]
Department of Chemistry, Yonsei University, 134 Sinchon-dong, Seodaemoon-gu, Seoul 120-749, Korea

Joost Beckers and Simon de Leeuw
Physical Chemistry and Molecular Thermodynamics, DelftChemTech, Delft University of Technology, Julianalaan 136, 2628 BL Delft, The Netherlands

Michael Thorpe[b)]
Physics and Astronomy Department, Michigan State University, East Lansing, Michigan 48824-1116

Mark A. Ratner
Department of Chemistry, Northwestern University, 2145 Sheridan Road, Evanston, Illinois 60208-3113

(Received 20 September 2004; accepted 8 February 2005; published online 29 April 2005)

We introduce a simple semiempirical anharmonic Kirkwood–Keating potential to model $A_xB_{1-x}C$-type semiconductors. The potential consists of the Morse strain energy and Coulomb interaction terms. The optical constants of pure components, *AB* and *BC*, were employed to fit the potential parameters such as bond-stretching and -bending force constants, dimensionless anharmonicity parameter, and charges. We applied the potential to finite temperature molecular-dynamics simulations on $Al_xGa_{1-x}As$ for which there is no lattice mismatch. The results were compared with experimental data and those of harmonic Kirkwood–Keating model and of equation-of-motion molecular-dynamics technique. Since the Morse strain potential effectively describes finite temperature damping, we have been able to numerically reproduce experimentally obtained optical properties such as dielectric functions and reflectance. This potential model can be readily generalized for strained alloys. © *2005 American Institute of Physics*.
[DOI: 10.1063/1.1883628]

I. INTRODUCTION

Understanding optical properties of group III-V pseudobinary random alloys is of major interest to research aimed at employing these materials, for instance, for the quantum cascade laser (QCL). QCL is in great demand for many laser-based application areas such as terabit optical data communications,[1] ultraprecision metrology,[2] spectroscopy,[3] and medical imaging.[4] This monolithic, mid-infrared supercontinuum semiconductor laser is inherently compact and provides high output power. Also, it is a unipolar laser[5] that is based on electron transitions within semiconductor quantum well nanostructures.[6,7] The emission structure of the QCL can be varied from a single quantum well to a complex chirped superlattice consisting of semiconductor layers of general formula $A_xB_{1-x}C$. Therefore, theoretical studies can greatly benefit the development and applications of QCL by designing a quantum well structure so that it can produce a desired and customized radiation profile.

$A_xB_{1-x}C$ random alloys typically adopt a zinc-blende crystal structure, with two sublattices (*AC* and *BC*). Due to the random substitution of a fraction of the *A*-type ions by *B* in one of the sublattices, the simple four-branch dispersion relation of the zinc-blende crystal no longer appears. Instead, we observe a complex mixture of pure system perturbed modes. Extensive experimental work has been devoted to describe vibrational states in this class of materials. The frequencies of the longitudinal-(LO) and transverse-(TO) optical modes of $Al_xGa_{1-x}As$ mixed crystals have been studied by Ilegems and Pearson[8] from the Kramers–Kronig analysis of infrared reflectance spectra followed by Raman spectroscopy study on the long-wavelength vibrational behavior.[9–12] Jusserand and Sapriel[13] measured the LO and TO mode behaviors with varying Al concentrations and thoroughly analyzed the line-shape asymmetry of these modes in terms of defect and anharmonicity. Optical properties of $Al_xGa_{1-x}As$ for Al concentrations have also been obtained using optical reflection techniques.[14]

In order to predict the optical properties of an alloy of arbitrary composition, a theoretical or computational method has also been used. The straightforward mean-field approximation has been shown to fail in producing correct spectra.[15,16] Alternatively, the coherent-potential approximation (CPA) model developed by Bonneville[17] as well as computational methods such as *ab initio* calculations has been more successful.[15,16,18] Baroni *et al.* have presented an *ab initio* model based on which they determined the dispersion of phonon branches in thin AlAs and GaAs films. Recently, Branicio *et al.* have performed molecular-dynamics (MD) simulations using an interaction potential and investigated structural, mechanical properties on $In_xGa_{1-x}As$ alloys.[19]

[a)]Author to whom correspondence should be addressed. Electronic mail: esim@yonsei.ac.kr
[b)]Current address: Department of Physics, Arizona State University, Tempe, AZ 85287-1504

However, these techniques are either computationally extremely demanding or difficult to generalize and apply to other alloys.

The main features of an experimental phonon spectrum are reproduced within the simple Kirkwood–Keating (valence-force) model.[20,21] This is a low-order expansion of the strain energy, with respect to atomic shifts relative to the perfect-crystal lattice sites, fitted to the elastic constants. However, there are considerable deviations in certain regions of the Brillouin zone. The major deviations occur at the zone-center (Γ) optical-phonon frequency ω_{TO}, which often tends to be overestimated (i.e., too large phonon force constant). The Kirkwood–Keating model gives a poor description on the flattening of the transverse-acoustic-phonon branch near the zone boundary (X).

It has been shown that the inclusion of further interaction terms can improve the calculated dispersion.[22,23] A six-parameter model satisfactorily has described the phonon frequencies of all four diamondlike crystals.[24] The general valence-force-field model has one two-body force α and three distinct three-body forces β, γ, and κ. The last two terms describe the correlation of angle distortion with the length change of one leg, and the correlation between the length changes of two neighboring bonds.

In this paper we propose a very simple semiempirical model potential modified from the Kirkwood–Keating potential, which reproduces the optical spectra of the $\mathrm{Al}_x\mathrm{Ga}_{1-x}\mathrm{As}$ random alloy that is taken here as an example material. The potential contains as few parameters as possible in order to facilitate the parameter fitting procedure and generalization to other alloys. The potential consists of terms that are directly related to atomic interactions. Moreover, the parameter fitting procedure is based on experimental data of pure components, which are usually known. We aim for a general model that can be used to predict optical properties of alloys of arbitrary composition. The $\mathrm{Al}_x\mathrm{Ga}_{1-x}\mathrm{As}$ alloy is a special case in the collection of possible pseudobinary alloys, because of the almost identical lattice constants of the pure components: AlAs and GaAs. As a consequence, there is virtually no length mismatch between the sublattices, which leaves only mass disorder. This simplifies the analysis, and the method will be equally valid for a wider range of materials.

This paper is organized as follows: In Secs. II and III, we introduce the potential and discuss how the various parameters can be fitted to experimental data of pure components, particularly GaAs and AlAs for a test case. We present results of dielectric and reflectance spectra of $\mathrm{Al}_x\mathrm{Ga}_{1-x}\mathrm{As}$ of varying composition x followed by concluding remarks in Sec. IV. The reflectance spectra are extremely sensitive to the position and shape of the peaks in the dielectric-response function and are therefore a good evaluation tool for our model.

II. MODEL

The total potential energy of the system is divided into the strain and Coulomb energy,

$$V_{\mathrm{total}} = V_{\mathrm{strain}} + V_{\mathrm{Coulomb}}. \tag{1}$$

We will discuss each term in details in Secs. II A and II B.

A. Anharmonic strain energy

It is known that the elastic constants of zinc-blende structure crystals in equilibrium are well described by Kirkwood–Keating's two-parameter model.[20,21] There have been many modifications to this harmonic model to improve the calculated dispersion curves by including further interaction terms. We introduce the anharmonic interaction by replacing the harmonic bond restoring interaction term in original Kirkwood–Keating model with the Morse potential using dimensionless anharmonicity parameter χ,

$$V_{\mathrm{strain}} = \sum_{\langle i,j\neq i\rangle} \frac{\alpha_{ij}}{2(\chi_{ij}/r_{ij}^0)^2}\{e^{-2(\chi_{ij}/r_{ij}^0)(r_{ij}-r_{ij}^0)} - 2e^{-\chi_{ij}/r_{ij}^0(r_{ij}-r_{ij}^0)} + 1\} + \sum_{\langle i,j\neq i,k\neq i,j\rangle} \frac{\beta_{ijk} r_{ij}^0 r_{ik}^0}{8}\left(\frac{\mathbf{r}_{ij}\mathbf{r}_{ik}}{r_{ij}r_{ik}} + \frac{1}{3}\right)^2. \tag{2}$$

The strain energy is taken to depend on the vector $\mathbf{r}_{ij}$ which connects nearest-neighbor lattice sites i and j. Index i runs over all atoms and j and k run over the four nearest neighbors of atom i in tetrahedral structure. r_{ij} is the distance between atoms i and j, while r_{ij}^0 is the equilibrium distance. In this expression, $\cos\theta_{ijk}=\mathbf{r}_{ij}\mathbf{r}_{ik}/r_{ij}r_{ik}$ is the scalar product between the two vectors connecting atom i with its neighbors j and k. The fraction $1/3$ inside the second bracket is the contribution from equilibrium tetrahedral angle 109° that gives $\cos(109)=-1/3$. In zinc-blende structure, the relationship between the equilibrium nearest-neighbor distance r^0 and the lattice constant a_0 is $a_0=4r^0/\sqrt{3}$. For simplicity, atomic indices of potential parameters will be omitted from this point forward such that we use α, β and χ instead of α_{ij}, β_{ijk}, and χ_{ij}. Both parameters α and β have the dimension of a force constant (N/m).

The first term in Eq. (2) represents the two-body central force interaction between nearest neighbors, i.e., the covalent bond between Ga–As or Al–As, while the second term describes the angular interaction between atom i and its two nearest neighbors j and k. The parameters α and β essentially describe the bond-stretching and bond-bending restoring forces. They are fitted to reproduce the elastic constants and phonon frequencies to those obtained experimentally.

B. Coulomb interaction

The bonds between group III-V elements can have significant polarity. The effective force constants α and β account only for the short-range part of the electrostatic forces, whereas the long-range electrostatic forces that arise for polarized bonds are neglected in the Kirkwood–Keating model. We add to Eq. (2) a term for the long-range electrostatic interactions, i.e., Coulomb interaction, between electrically charged ions,

$$V_{\text{Coulomb}} = \frac{1}{4\pi\varepsilon_0\varepsilon_\infty}\sum_{\langle i,j\neq i\rangle}\frac{q_i q_j}{r_{ij}}, \tag{3}$$

where ε_0 is the permittivity of vacuum, ε_∞ is the high-frequency dielectric constant, and q_i is the charge of ion i.

The effect of long-range interactions on the strain energy of group III-V compounds is expected to be small, but the long-range forces are essential for correct description of the phonon dispersion. They are, for instance, responsible for the splitting of the LO- and TO-phonon frequencies at the Brillouin-zone center. The LO displacement produces macroscopic ionic polarization. A corresponding macroscopic electric field produces an additional restoring force, giving rise to a LO frequency shift.

The Ewald summation method[25] is used to avoid anomalies from a Coulomb interaction cutoff radius. We use a velocity Verlet time integration scheme with a time step of 2 fs. All simulations are performed at constant volume. The MD runs are kept at constant temperature by a Nosé extended system thermostat. Periodic boundary conditions are imposed for all simulations. Since the atoms in the group III-V alloy are polar, we intentionally use an uneven-surface rectangular sample to avoid the macroscopic electrostatic field of a bulk sample. The usual periodic boundary is applied and the interaction cutoff distance at 8.5 Å is used for simulation efficiency. The total number of atoms is 480 with 60 unit cells.

III. OPTICAL PROPERTIES OF $Al_xGa_{1-x}As$

The potential parameters in Eqs. (2) and (3) depend on the type of atoms in a random alloy of interest. As an example we take an $Al_xGa_{1-x}As$ system, which has the advantage that there is almost no length mismatch between AlAs and GaAs sublattices. The potential parameters of the pure GaAs and AlAs are very similar in many empirical model potentials.[26,27] We therefore expect that the parameters for AlAs and mixed alloys will be close to pure GaAs. The model can be generalized for more complex systems with lattice strain.

Experimental data of the pure systems GaAs and AlAs, which are well available from literature,[28,29] are used to fit the potential parameters. These data include the dispersion relation of phonon frequencies, refractive index, extinction coefficient, dielectric spectrum, and reflectance. Both analytical expressions and empirical fitting methods are used. The empirical methods amount to testing a trial parameter set with the equation-of-motion molecular dynamics[30] (EQM-MD) or standard MD at room temperature and adjusting the parameters until they produce fair agreement with experimental results. The potential parameters α and β are fitted to match the GaAs optical-phonon bands, using two analytical and one empirical relations between these parameters and the phonon frequencies. The anharmonicity parameter, χ, is fitted to the reflectance spectrum.

We will first consider parameters for the GaAs side and later discuss AlAs side in this section. The optical-phonon frequency at the zone center, i.e., $k=0$, ω_0, of a non-Coulombic zinc-blende structure, can be derived from a harmonic approximation of the potential Eq. (2). For a Coulombic system, ω_0 can be calculated from the LO- and TO-phonon frequencies (ω_{LO} and ω_{TO}) given by[27]

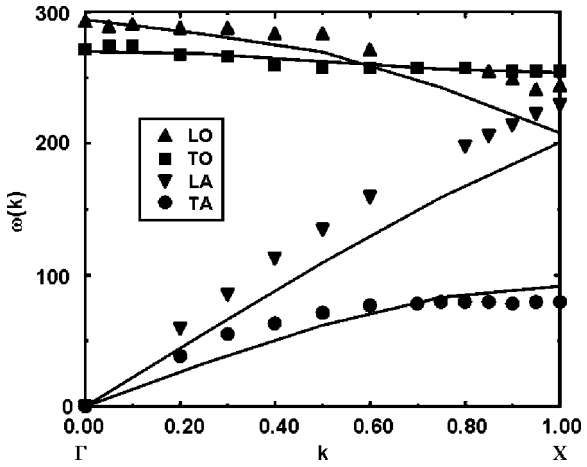

FIG. 1. Phonon-dispersion curve for pure GaAs(100) with experimental data (symbols) reproduced from Bilz and Kress (Ref. 31). The solid lines are obtained from molecular-dynamics simulations at room temperature. X corresponds to the Brillouin-zone boundary, while Γ to zone center. The calculated TO-phonon frequencies agree well with the experiment for the entire zone, since we fit the β angular parameter to the relationship Eq. (3).

$$\omega_0^h = \frac{2}{3}\omega_{\text{TO}} + \frac{1}{3}\omega_{\text{LO}} = \sqrt{\frac{4}{3\mu}\left[\alpha + \frac{16}{9}\beta\right]}, \tag{4}$$

where μ is the reduced mass. The superscript h indicates that the phonon frequency was obtained using the harmonic approximation. The parameter β mainly controls the downshift of the TO band within the Brillouin zone,

$$\Delta\omega_{\text{TO}} = \omega_{\text{TO}}(\Gamma) - \omega_{\text{TO}}(X). \tag{5}$$

We found, by empirical methods, a linear dependence of the TO shift on parameter β. This enables independent determination of β. Hence, we first fit the angular interaction parameter β to reproduce the width of the GaAs TO dispersion curve, while using approximate values for α and q. The phonon-dispersion spectrum can be determined in the usual way. For GaAs, a best fit of 15-cm^{-1} shift was found using $\beta = 5.7$ N/m.[31]

When we introduce ionic charges, the LO and TO bands in the dispersion relation split, where the LO phonon shifts to a higher frequency and that of TO is shifted lower. This LO-TO Coulomb splitting has been studied for many systems.[30,32] The difference between the LO and TO frequencies is related to the plasma frequency, ω_p, which, for pure crystals, can be computed from the Lyddane–Sachs–Teller relation[33]

$$\omega_p^2 = \omega_{\text{LO}}^2 - \omega_{\text{TO}}^2 = \frac{1}{V\varepsilon_0\varepsilon_\infty}\sum_i \frac{q_i^2}{m_i}, \tag{6}$$

where V is the volume of the system and m_i is the mass of ion i. The parameters α and q are computed from Eqs. (4) and (6) and previously determined β,[34,35] $\omega_{\text{LO}} = 270$ cm^{-1}, $\omega_{\text{TO}} = 295$ cm^{-1}, and $\omega_0 = 279$ cm^{-1}. We found that $\alpha = 115$ N/m and $q = 2.27e$. Simulations with this set of parameters resulted in the dispersion relation shown in Fig. 1. The

dispersion relations are in reasonable agreement with experiment despite the simplicity of the model. The vibration dispersion spectrum of this zinc-blende crystal structure contains six branches, three optical and three acoustic branches. Both the optical and the acoustic branches consist of two transverse and one longitudinal modes. The optical branches are pairwise degenerate. The Coulomb splitting of the optical modes is clearly visible. The longitudinal branches deviate from the experimental data near the zone boundary. We expect that this deviation will have only a small effect on most of the optical spectra that mainly couple to the TO modes. The data taken from the dispersion curves are $\omega_{\mathrm{TO}}(0) = 270\ \mathrm{cm}^{-1}$, $\omega_{\mathrm{LO}}(0) = 294.3\ \mathrm{cm}^{-1}$, and $\omega_{\mathrm{TO}}(0) - \omega_{\mathrm{TO}}(1) = 16.1\ \mathrm{cm}^{-1}$. These are in agreement with experiment and with our analytical calculations.

Next, the anharmonicity parameter χ is fitted to the GaAs reflectance spectrum. The reflectance is a function of the complex dielectric function $\varepsilon(\omega)$, which we need to calculate first. The dielectric function is obtained from the current autocorrelation function (CACF), computed from a MD run. The imaginary part of the dielectric function is computed with a Gaussian screening function as follows:

$$\varepsilon''(\mathbf{k},\omega) = \frac{2\pi}{V\omega}\frac{2}{\pi}\int_0^T dt\,\cos(\omega t)\exp[-\sigma(t/T)^2] \times\left\langle \sum_i q_i \mathbf{v}_i(t)\sum_j q_j \mathbf{v}_j(0)\right\rangle, \tag{7}$$

where $\mathbf{v}_i$ is the velocity vector of an ith atom. The angular brackets denote the usual ensemble averaging. The Gaussian damping factor σ was set to 3.0. The real part, $\varepsilon'(\mathbf{k},\omega)$, can be obtained by using corresponding sine transform, or through Kramers–Kronig transformation of $\varepsilon''(\mathbf{k},\omega)$. Then the reflectance, $R(\omega)$, is computed from $\varepsilon(\omega)$ through

$$R(\omega) = \left|\frac{1-\sqrt{\varepsilon(\omega)}}{1+\sqrt{\varepsilon(\omega)}}\right|^2. \tag{8}$$

The reflectance is a function of the LO and TO frequencies and, as we found, is also highly sensitive to the peak widths. These peak widths, or second moments of the dielectric response, are related to the decay of the CACF. A fast decay causes a broad peak in $\varepsilon(\omega)$. This CACF decay, or the damping in the TO modes, is mainly due to anharmonicity effects, since the anharmonic terms enhance the coupling to other modes and the dispersion of phonon energy. The reflectance maximum is therefore a good measure of the degree of anharmonicity in the system and a proper quantity for fitting the value of χ. This damping effect of anharmonicity on the reflectance is clearly seen in Fig. 2. EQM-MD technique gives the $T=0$ K limit, where the higher-order terms in the potential are negligible and the system is essentially harmonic. This produces a region of 100% reflectance: the Reststrahlen band between the LO and TO frequencies. At finite temperature, if anharmonic effects are included, this 100% reflection band is reduced by damping and coupling to other modes. The Kirkwood–Keating potential is weakly anharmonic due to the angular terms and the MD simulation at 300 K produces a 97% reflectance maximum. This damping

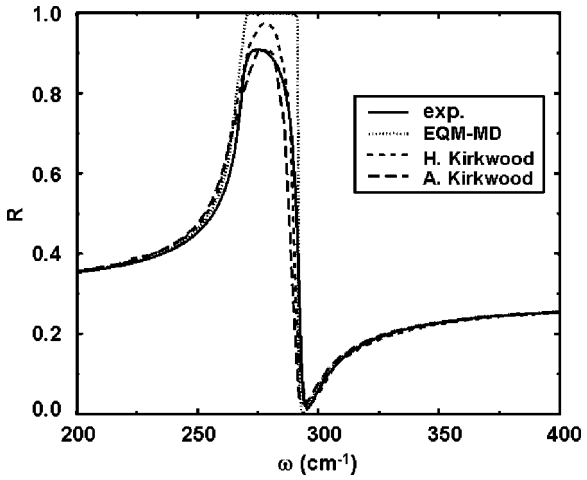

FIG. 2. Reflectance of GaAs using various simulation methods. The solid line represents experimental result from Ref. 35, the dotted line is obtained from equation-of-motion molecular-dynamics simulation, and the dashed and long-dashed lines are from room-temperature molecular-dynamics simulations. Harmonic Kirkwood–Keating model has been used for the dashed line while anharmonic Kirkwood–Keating model has been used for the long-dashed line. The equation-of-motion technique represents $T=0$ condition. The anharmonic Morse potential gives a better fit to the experimental data than the harmonic bond-stretch potential by including physical damping effects.

is less than that observed in experiment. Although the angular terms introduce anharmonicity to a certain extent, the Kirkwood–Keating model needs an additional damping factor to mimic a real system. This is the reason we added anharmonicity by introducing the Morse potential in the strain energy. The parameter χ controls the degree of anharmonicity. Using a χ of 1.36, the maximum reflectance of GaAs is reduced to the experimental value of 90%, as shown in Fig. 2. In principle, the ω_0^h can depend on χ. We therefore recalculated this frequency after adjusting χ. For $\mathrm{Al}_x\mathrm{Ga}_{1-x}\mathrm{As}$, the effect was negligible, but for other compounds one may need to rewrite the expression of phonon frequency such that χ is included.

For $\mathrm{Al}_x\mathrm{Ga}_{1-x}\mathrm{As}$, the ionic charges are constant over the composition range, but the high-frequency dielectric constant ε_∞ varies. Its value is estimated from the Clausius–Mossotti equation[36]

$$\frac{\varepsilon-\varepsilon_\infty}{\varepsilon+2\varepsilon_\infty} = \frac{4\pi}{3V}(N_{\mathrm{AlAs}}\eta_{\mathrm{AlAs}} + N_{\mathrm{GaAs}}\eta_{\mathrm{GaAs}}), \tag{9}$$

where N_{AlAs} (N_{GaAs}) is the number density of AlAs(GaAs). The polarizabilities η are determined from experimental result of ε_∞ for the pure systems: $\varepsilon_\infty(\mathrm{GaAs}) = 10.88$ and $\varepsilon_\infty(\mathrm{AlAs}) = 8.16$.

The parameters for the AlAs are kept identical to the GaAs except for a somewhat larger bond-stretch parameter α. This is done to shift the AlAs dispersion to larger wave numbers and get a better overlap for the reflectance data. The optimized set of parameters is listed in Table I. The ionic charges appear rather large due to the relative dielectric constant in the form of $q^{\mathrm{eff}} = q/\sqrt{\varepsilon_\infty}$ that is used in the Coulomb term in Eq. (3). Correcting for the high-frequency dielectric constants yields charges of $q_{\mathrm{Ga}}^{\mathrm{eff}} = -0.69$ and $q_{\mathrm{Al}}^{\mathrm{eff}} = -0.79$ for the pure systems.

TABLE I. Potential parameters for $Al_xGa_{1-x}As$.

	r_0(Å)	α(N/m)	β(N/m)	χ	$q_{As}^{eff}[q(e)]$
GaAs	2.47	115	5.7	1.36	0.69 [2.27]
AlAs	2.47	119	5.7	1.36	0.79 [2.27]

Finally, we discuss the optical properties of $Al_xGa_{1-x}As$ with varying Al composition. It has been known that III-V semiconductor alloys show a two-mode behavior,[37] exhibiting two sets of phonon mode where the phonon frequencies are close to those of pure components. Figure 3 shows the dielectric function of $Al_xGa_{1-x}As$ calculated from MD runs at 300 K with several values of Al composition. Clearly the dielectric function displays the two-mode behavior, which agrees well with experimental observation.[38] As the mole fraction of Al increases, starting with pure GaAs, the dielectric function develops a peak near the pure AlAs peak (hereafter, AlAs-like peak). The peak positions and widths (second moment) of $\varepsilon''(\omega)$ as functions of the Al mole fraction are plotted in Fig. 4(a). The GaAs-like peak shifts to longer wavelength (redshift by approximately 20 cm^{-1}) as Al composition increases, while the AlAs-like one shifts to shorter wavelength (blueshift by approximately 10 cm^{-1}). This means that both the AlAs- and GaAs-like peaks shift to longer wavelengths as its mole fraction decreases.[39] The peak width is the largest, as expected, when an alloy is an equal mixture of GaAs and AlAs and becomes narrow as one component dominates. Note also that the peaks are asymmetric. As Al composition fraction increases, GaAs-like peaks become asymmetric; short-wavelength side on the right becomes broader than long-wavelength side on the left. This behavior is also observed in AlAs-like peaks where the lower-frequency side is broader than the higher-frequency side. The integral of $\varepsilon''(\omega)$ spectrum can be related to the plasma frequency through the sum rule,[30]

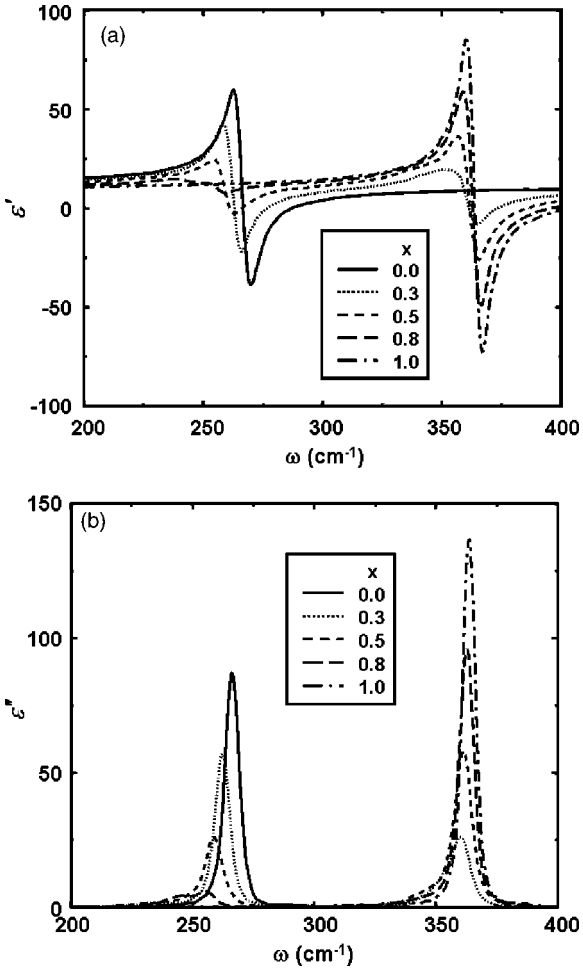

FIG. 3. (a) Real and (b) imaginary parts of dielectric function ε' of $Al_xGa_{1-x}As$ pseudobinary alloy for various Al compositions x. Notice the two-mode behavior of the dielectric function which agrees with experimental observation in Ref. 38.

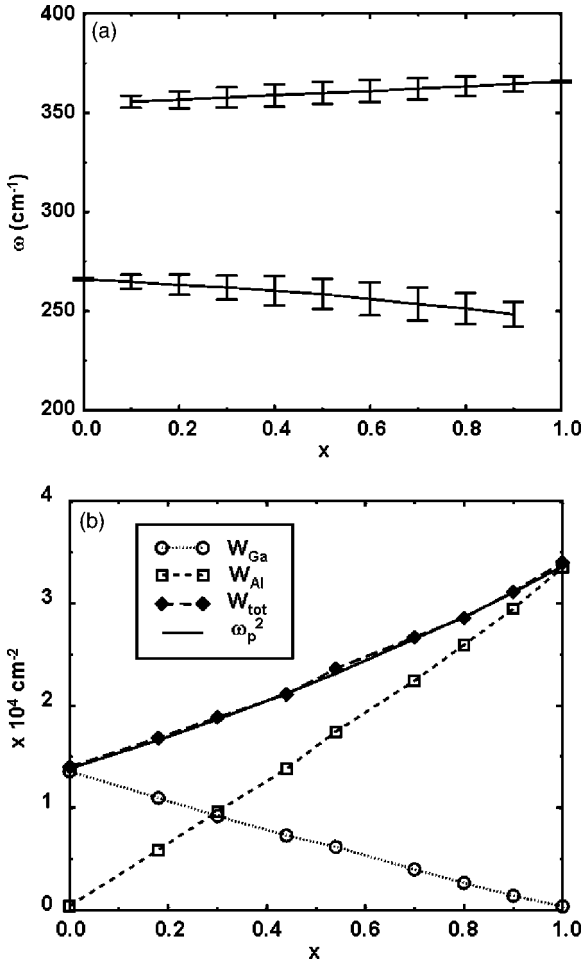

FIG. 4. (a) Peak positions and second moments of $\varepsilon''(\omega)$ of $Al_xGa_{1-x}As$ pseudobinary alloy for various Al compositions x. Note that the error bar represents full width at half maximum (FWHM) of each peak. The results are from room-temperature molecular-dynamics runs using the potential parameters shown in Table I. The two-mode behavior is clearly seen throughout all composition ranges. (b) Weights of the Ga- and Al-type peaks of $\varepsilon''(\omega)$ as a function of Al fraction x. The sum of the two weights increases following ω_p^2 (solid line), calculated from Eq. (10), thus satisfying the sum rule. It should be noted that the almost linear behavior of ω_p^2 is coincidental.

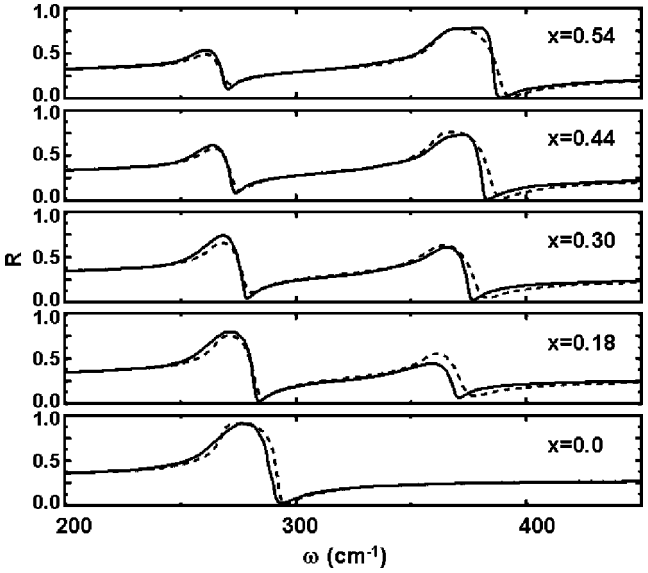

FIG. 5. Reflectance of $Al_xGa_{1-x}As$ compared with experimental results. The mole fraction of Al decreases from the top to the bottom panel; $x=0.54, 0.44, 0.30, 0.18, 0.0$. The solid lines are from 300 K molecular-dynamics simulations and the dashed lines are taken from Ref. 35. Note that the reflectance peak shifts as the composition changes. The results of simulated reflectance shown here are calculated with Eq. (8) using the dielectric functions screened with Gaussian functions that appear in Eq. (7).

$$\frac{2}{\varepsilon_\infty \pi}\int_0^\infty d\omega\omega\varepsilon''(\omega) = \omega_p^2. \tag{10}$$

Since the two peaks are well separated, by distinguishing Ga- and Al-type peaks of $\varepsilon''(\omega)$ and defining the weights of each peak accordingly, in Fig. 4(b) one can see that this weight gradually shifts from GaAs- to AlAs-like peak as Al composition increases. The sum of the two weights increases following the plasma frequency, thus satisfying the sum rule. It should be noted that the almost linear behavior of ω_p^2 is coincidental. Although, in general, the strength of each mode is proportional to the mole fraction of the corresponding component, we observed that Al-type peak has larger weight even when the Al fraction is less than half. Overemphasis on the Al-type peak is caused by the neglected site dependence of Al charges.[39] The weights of the two peaks are the same when Al fraction is 0.3.

Figure 5 compares calculated and experimentally measured reflectance spectrum of $Al_xGa_{1-x}As$. The reflectance peak shifts as the composition changes displaying the two-mode behavior. The results of simulated reflectance shown here were calculated with Eq. (8) using dielectric functions screened with Gaussian functions in Eq. (7).

IV. CONCLUSION

Using a very simple semiempirical anharmonic Kirkwood–Keating potential with parameters fitted to the pure components, GaAs and AlAs in this paper, we have been able to reproduce optical properties such as dielectric functions and reflectance spectra of mixed compounds. We found that the reflectance is highly sensitive to higher order terms in the potential, in particular, to the degree of anharmonicity of the stretch term. It has been shown that this anharmonicity is essential for a correct reflectance spectrum at finite temperature. The dimensionless anharmonicity parameter introduced into the harmonic Kirkwood–Keating model provided effective damping to mimic a real system at finite temperature.

The model can easily be extended to other systems of semiconductor alloys by taking into account the compositional dependence on parameters such as the lattice constants, dielectric constants, and charges. While lattice-matched layers can be used for long wavelength quantum well lasers, strain balancing has been shown to be a viable technique to realize short-wavelength QCLs. Highly strain-balanced heterostructure quantum wells, such as $In_xGa_{1-x}As$, can provide short-wavelength lasers with high conduction-band offset and minimal leakage current. Intensive studies on $In_xGa_{1-x}As$ using the anharmonic Kirkwood–Keating potential introduced in this article are currently under progress.

ACKNOWLEDGMENT

This work was supported by Korea Research Foundation Grant No. (KRF-2004-003-C00105).

[1] B. C. Collings, M. L. Mitchell, L. Boivin, and W. H. Knox, Opt. Photonics News **11**, 31 (2000).
[2] D. J. Jones, S. A. Diddams, J. K. Ranka, A. Stentz, R. S. Windeler, J. L. Hall, and S. T. Cundiff, Science **288**, 635 (2000).
[3] H. I. Shiff, G. I. Mackay, and J. Bechara, in *Air Monitoring by Spectroscopic Techniques*, edited by M. W. Sigrist (Wiley Interscience, New York, 1994), p. 239.
[4] P. Y. Han, G. C. Cho, and X.-G. Zhang, Opt. Lett. **25**, 242 (2000).
[5] J. Faist, F. Capasso, D. L. Sivco, C. Sirtori, A. L. Hutchinson, and A. Y. Cho, Science **264**, 553 (1994).
[6] M. Razeghi and S. Slivken, Opto-Electron. Rev. **11**, 85 (2003).
[7] C. Gmachl, D. L. Sivco, R. Colombelli, F. Capasso, and A. Y. Cho, Nature (London) **415**, 883 (2002).
[8] M. Ilegems and G. L. Pearson, Phys. Rev. B **1**, 1576 (1970).
[9] R. Tsu, H. Kawamura, and I. Esaki, in *Proceedings of the International Conference on the Physics of Semiconductors*, edited by M. Miasek (PWN-Polish Scientific, Warsaw, 1972), Vol. 2, p. 1135.
[10] G. Abstreiter, E. Bauer, A. Fischer, and K. Ploong, Appl. Phys. **16**, 345 (1978).
[11] T. Yuasa, S. Naritsuka, M. Mannoh, K. Shinozaki, K. Yamanaka, Y. Nomura, M. Mihara, and M. Ishii, Phys. Rev. B **33**, 1222 (1986).
[12] D. Kirillov, Y. Chai, C. Webbs, and G. Davis, J. Appl. Phys. **59**, 231 (1986).
[13] B. Jusserand and J. Sapriel, Phys. Rev. B **24**, 7194 (1981).
[14] D. E. Aspnes, S. M. Kelso, P. A. Logan, and R. Bhat, J. Appl. Phys. **60**, 756 (1986).
[15] B. Jusserand, D. Paquet, and F. Mollot, Phys. Rev. Lett. **63**, 2397 (1989).
[16] B. Jusserand, F. Mollot, R. Planel, E. Molinari, and S. Baroni, Surf. Sci. **267**, 171 (1992).
[17] R. Bonneville, Phys. Rev. B **24**, 1987 (1981).
[18] S. Baroni, S. de Gironcoli, and P. Giannozzi, Phys. Rev. Lett. **65**, 84 (1990).
[19] P. S. Branicio, J. P. Rino, F. Shimojo, R. K. Kalia, A. Nakano, and P. Vashishta, J. Appl. Phys. **94**, 3840 (2003).
[20] J. G. Kirkwood, J. Chem. Phys. **7**, 506 (1939).
[21] P. N. Keating, Phys. Rev. **145**, 637 (1966).
[22] D. Vanderbilt, S. H. Taole, and S. Narasimhan, Phys. Rev. B **40**, 5657 (1989).
[23] H. Rücker and M. Methfessel, Phys. Rev. B **52**, 11059 (1995).
[24] R. Tubino, L. Piesri, and G. Zerbi, J. Chem. Phys. **56**, 1022 (1972).
[25] P. Ewald, Ann. Phys. **64**, 253 (1921).
[26] S. Baroni, P. Gianozzi, and A. Testa, Phys. Rev. Lett. **58**, 1861 (1987).
[27] Y. Cai and M. F. Thorpe, Phys. Rev. B **46**, 15879 (1992).
[28] In *Semiconductors: Group IV Elements and III-V Compounds*, edited by R. Poerschke and O. Madelung (Springer, New York, 1991).
[29] In *Handbook of Optical Constants of Solids*, edited by E. D. Palik (Aca-

demic, Boston, 1985).
[30]M. F. Thorpe and S. W. de Leeuw, Phys. Rev. B **33**, 8490 (1986).
[31]H. Bilz and W. Kress, in *Phonon Dispersion Relations in Insulators*, Springer Series in Solid State Sciences Vol. 10 (Springer, Berlin, 1979), p. 105.
[32]F. L. Galeener and G. Lucovsky, Phys. Rev. Lett. **37**, 1474 (1976).
[33]R. J. Elliott, J. A. Krumhansl, and P. L. Leath, Rev. Mod. Phys. **46**, 465 (1974).
[34]B. Jusserand, D. Paquet, and F. Mollot, Phys. Rev. Lett. **63**, 2397 (1981).
[35]O. K. Kim and W. G. Spitzer, J. Appl. Phys. **50**, 4362 (1979).
[36]N. Ashcroft and N. D. Mermin, *Solid State Physics* (Holt, Rinehart and Winston, New York, 1976).
[37]I. F. Chang and S. S. Mitra, Adv. Phys. **20**, 359 (1971).
[38]J.-L. Guyaux, P. A. Thiry, R. Sporken, and R. Caudano, Phys. Rev. B **48**, 4380 (1993).
[39]M. Bernasconi, L. Colombo, L. Miglio, and G. Benedek, Phys. Rev. B **43**, 14447 (1991).